

# One-step synthesis of Mn-doped MIL-53(Fe) for synergistically enhanced generation of sulfate radicals towards tetracycline degradation

Jun Yu <sup>a,b,1</sup>, Jiao Cao <sup>a,b,1</sup>, Zhaohui Yang <sup>a,b,\*</sup>, Weiping Xiong <sup>a,b,\*</sup>, Zhengyong Xu <sup>c</sup>, Peipei Song <sup>d</sup>, Meiyong Jia <sup>a,b</sup>, Saiwu Sun <sup>a,b</sup>, Yanru Zhang <sup>a,b</sup>, Juan Zhu <sup>e</sup>

<sup>a</sup> College of Environmental Science and Engineering, Hunan University, Changsha 410082, PR China

<sup>b</sup> Key Laboratory of Environmental Biology and Pollution Control (Hunan University), Ministry of Education, Changsha 410082, PR China

<sup>c</sup> Science and Technology Service Center of Hunan Province, Changsha 410128, PR China

<sup>d</sup> College of Resources and Environment, Key Laboratory of Agricultural Environment, Shandong Agricultural University, Tai'an 271000, PR China

<sup>e</sup> Hunan Xinheng Environmental Technology Co Ltd, Changsha 410005, PR China

## HIGHLIGHTS

- Mn-MIL-53(Fe) was synthesized by one-step solvothermal method.
- The obtained Mn-MIL-53(Fe) could efficiently activate peroxymonosulfate (PMS).
- Reaction parameters of Mn-MIL-53(Fe)/PMS system for TC degradation were optimized.
- Possible mechanism of tetracycline (TC) degradation and TC degradation pathway were investigated proposed.
- The Mn-MIL-53(Fe) system exhibited high efficiency in actual water.

## GRAPHICAL ABSTRACT



## ARTICLE INFO

### Article history:

Received 23 April 2020

Revised 8 July 2020

Accepted 9 July 2020

Available online 15 July 2020

### Keywords:

Peroxymonosulfate activation

Mn-doped

MIL-53(Fe)

Tetracycline

One-step solvothermal synthesis

## ABSTRACT

Herein, Mn-doped MIL-53(Fe) were fabricated via one-pot solvothermal method and used for peroxymonosulfate (PMS) activation towards tetracycline (TC) degradation from aqueous solution. The characterizations of SEM, FTIR and XRD were utilized to reveal the morphology and structure of the materials. The results showed that Mn-MIL-53(Fe)-0.3 displayed the optimal catalytic performance, the removal efficiency of TC could reach 93.2%. Moreover, the catalytic activity of Mn-MIL-53(Fe) towards TC under different initial pH values, co-existing anions ( $\text{Cl}^-$ ,  $\text{CO}_3^{2-}$  and  $\text{SO}_4^{2-}$ ) and humic acid (HA) were investigated. The results of thermodynamic experiment suggested that the catalytic process was endothermic. In addition, integrated with capture experiments results and the characterization results of electron paramagnetic resonance (EPR), which revealed that  $\text{SO}_4^{\cdot-}$  and  $\text{HO}^{\cdot}$  were the reactive radicals involving in the reaction. More importantly, the possible activation mechanism was discussed in detail based on the X-ray photoelectron spectroscopy results. The active species were generated by the active sites of Fe(II) and Mn(II) on Mn-MIL-53(Fe) effectively activated PMS. Furthermore, the degradation intermediates and possible degradation pathway were investigated by LC-MS. Finally, the catalyst also showed good performance in actual wastewater and demonstrated good recyclability. The Mn-MIL-53(Fe)/PMS system exhibited a promising application prospect for antibiotic-containing waste water treatment.

© 2020 Elsevier Inc. All rights reserved.

\* Corresponding authors at: College of Environmental Science and Engineering, Hunan University, Changsha, Hunan 410082, PR China.

E-mail addresses: [yzh@hnu.edu.cn](mailto:yzh@hnu.edu.cn) (Z. Yang), [xiongweiping@hnu.edu.cn](mailto:xiongweiping@hnu.edu.cn) (W. Xiong).

<sup>1</sup> These authors contribute equally to this article.

## 1. Introduction

So far, antibiotics have been broadly used in the fields of medicine, animal husbandry and fish farming as antimicrobial agents [1]. However, the widespread utilization and discharge of antibiotics, such as tetracycline (TCs), enables them can be constantly discovered in medical wastewater, domestic sewage, and even surface water. The residue of antibiotics and their derivatives not only cause serious environmental issues, but also have a potential impact on human health [2,3]. However, conventional treatment is difficult to degrade antibiotic residues. Therefore, employ low-cost and efficient methods to eliminate the antibiotics from aquatic environment is significance.

In the past few decades, a variety of methods for removing antibiotic contaminants from aquatic environment have been extensively investigated, including electrodegradation [4,5], anaerobic digestion [6,7] and photocatalytic degradation [8–10] etc. Among these methods, advanced oxidations processes (AOPs) shows excellent potential for antibiotics degradation, due to the generated radicals with high oxidative efficiency [11]. AOPs with sulfate radical ( $\text{SO}_4^-$ ) as the main free radical has been extensively explored for its high redox potential, high oxidation selectivity and strong oxidation capacity, which makes it has great application potential in wastewater treatment [12].

The generation of sulfate radical ( $\text{SO}_4^-$ ) can be achieved by the transition metals activation of peroxymonosulfate, as show in Eqs. (1) and (2). Recently, the heterogeneous catalytic system which couples of transition metals (Co, Mn and Fe) and peroxymonosulfate (PMS) has been shown to degrade antibiotics efficiently [13,14]. Among them, the  $\text{Co}^{2+}$ /PMS system showed excellent efficiency in the removal of antibiotics, and the system is stable at a wide pH range [15,16]. However, the  $\text{Co}^{2+}$  leached by Co-containing catalysts may cause more serious damage to the environment, which seriously restricts its practical application in water treatment. Fortunately, Mn-based catalysts also can effectively eliminate antibiotic contaminants from aquatic environment and  $\text{Mn}^{2+}$  is relatively more eco-friendly than  $\text{Co}^{2+}$ . In general, transition metals at redox potential can react more easily with PMS, thus facilitating the formation of active radicals [17,18]. Among Co, Mn and Fe, Co has the highest standard redox potentials of 1.92 V, and the redox potentials of Mn and Fe are 1.54 V and 0.77 V. Therefore, Co-based catalyst is more effective than Mn-based and Fe-based catalysts in activating PMS for antibiotics degradation. However, since the leached  $\text{Co}^{2+}$  is relatively more toxic than  $\text{Mn}^{2+}$  and  $\text{Fe}^{2+}$ , Mn-based catalysts and Fe-based catalysts are more eco-friendly catalysts. Thus, it is imperative to develop Mn-based and Fe-based catalysts with excellent properties for antibiotics degradation [19,20].



In recent years, metal organic frameworks (MOFs) has engaged great attention of researchers. MOFs as a porous material which are formed through the connection between organic ligands and inorganic units by strong bonds [21,22]. Due to its special high surface area, large pore volume, easy tunability and easy to be modified, MOFs have showed great potential applications in adsorption, catalysis and gas storage [23,24]. In addition, MOFs exhibited better performance than traditional materials for organic pollutants removal. For instance, Li et al. synthesized MIL100-MIP which can accurately identify and catalyze diethyl phthalate (DEP) degradation from wastewater [25]. Their study explored that the selective removal efficiency of MIL100-MIP to DEP was almost 6 times

than  $\text{Fe}^0$  and 1.5 times than activated carbon (AC). Liao et al. [26] obtained MIL-88A-Fe with rod-shaped structure by one-step solvothermal method for the removal of phenol, which was more convenient than high temperature calcination for the synthesis of biochar-based materials. Cao et al. [27] investigated that Co-doped UiO-66 was effective in removing TC in solution due to its high specific surface area and multiple active sites. Therefore, it is necessary to explore efficient MOFs-based catalysts for the removal of organic pollutants. Among numerous MOFs materials, MIL-53(Fe) has the advantages of stable structure, easy to modified and multifunctional, which enables it been widely investigated by many researchers [28]. Furthermore, the metal centers of  $\text{Fe}^{3+}/\text{Fe}^{2+}$  showed better catalytic performance. In general, the active metal center of MOFs is the main reason for its catalytic activity. MOFs with multiple metal centers may exhibit better catalytic performance than MOF with isolated metal centers [29]. Therefore, transitional metal-doped modification can obviously enhance the particular activity of MOFs and have attracted numerous attention in recent years [30].

Hence, in this work, we focus on doping MIL-53(Fe) with  $\text{Mn}^{2+}$ . Mn-doped MIL-53(Fe) series with different Mn contents were synthesized for catalytic degradation of TC from aqueous solutions. What's more, the removal efficiency of TC by Mn-MIL-53(Fe)/PMS systems under different pH values, temperature, co-existing ions, and humic acid were evaluated. Besides, the possible mechanism of Mn-MIL-53(Fe) activation of PMS to generate active radicals has been obtained by XPS, EPR and radical capture experiments. Furthermore, the reusability of Mn-MIL-53(Fe) was assessed and the degradation intermediate and possible degradation pathway were investigated by LC-MS. The improvement of TC removal efficiency indicated that a feasible strategy was adopted to enhance the catalytic performance of MOFs.

## 2. Materials and methods

### 2.1. Chemicals

Iron(III) chloride hexahydrate ( $\text{FeCl}_3 \cdot 6\text{H}_2\text{O}$ , 99.0%), manganese (II) chloride ( $\text{MnCl}_2 \cdot 4\text{H}_2\text{O}$ , 99.0%), *N,N*-Dimethylformamide (DMF), terephthalic acid ( $\text{H}_2\text{BDC}$ , 99.0%), tetracycline (TC), sodium chloride (NaCl), sodium sulfate ( $\text{Na}_2\text{SO}_4$ ), sodium carbonate ( $\text{Na}_2\text{CO}_3$ ), humic acid (HA), anhydrous ethanol, methanol and tertiary butanol (TBA) were obtained from Sinopharm Chemical Reagent Co., Ltd. (Shanghai, China). Potassium monopersulfate triple salt (PMS, 42%–46%  $\text{KHSO}_5$  basis) were purchased from Macklin Biochemical Co., Ltd. (Shanghai, China). The reagents mentioned above were all analytical grade and have not been further purified.

### 2.2. Preparation of samples

MIL-53(Fe) was obtained with DMF as solvent by one-step solvothermal method [31]. Typically, put  $\text{FeCl}_3 \cdot 6\text{H}_2\text{O}$ ,  $\text{H}_2\text{BDC}$  and DMF into a beaker and stirred at room temperature until clarify, where their molar ratio was 1:1:280. Subsequently, poured the solution into a 100 mL Teflon-lined steel reactor and put in an oven statically for 15 h under the condition of 150 °C. After the temperature of the solution in the reactor decreased to room temperature, it was centrifuged and washed several times by DMF and anhydrous ethanol. And the yellow product of MIL-53(Fe) was obtained. Finally, the obtained yellow product was placed in a vacuum drying oven and dried at 60 °C overnight.

The preparation of Mn-MIL-53(Fe) was similar with MIL-53(Fe). Typically, 0.674 g  $\text{FeCl}_3 \cdot 6\text{H}_2\text{O}$ , 0.415 g  $\text{H}_2\text{BDC}$  and 56 mL DMF were stirred evenly on the magnetic agitator. Proper amount of

MnCl<sub>2</sub>·4H<sub>2</sub>O (the molar ratio of MnCl<sub>2</sub>·4H<sub>2</sub>O and FeCl<sub>3</sub>·6H<sub>2</sub>O were 1:0.3, 1:0.5, 1:1, 1:2 and 1:3, respectively) was added in above solution. After stirring, transferred the solution into Teflon-lined steel autoclave and put in an oven statically for 15 h under the condition of 150 °C. After the temperature of the solution in the autoclave decreased to room temperature, it was separated by centrifugation and washed several times by DMF and anhydrous ethanol. Finally, the obtained product was placed in a vacuum drying oven and dried at 60 °C overnight. The obtained powder was named as Mn-MIL-53(Fe)-X (X = 0.3, 0.5, 1, 2 and 3, which represents for the MnCl<sub>2</sub>·4H<sub>2</sub>O: FeCl<sub>3</sub>·6H<sub>2</sub>O mole ratio).

The characterization methods and experiment methods were described in [Supporting Information \(SI\)](#).

### 3. Results and discussion

#### 3.1. Characterizations

The morphological structures of synthesized samples were analyzed by scanning electron microscope (SEM). As the SEM images displayed ([Fig. 1a](#)), the particles of MIL-53(Fe) exhibited a regular hexagonal pyramid-like shape with a uniform size. It could be observed from [Fig. 1b](#) that the addition of Mn<sup>2+</sup> obviously affected the morphological structure of MIL-53(Fe). [Fig. 1b](#) showed that the morphology of Mn-MIL-53(Fe)-0.3 presented a double-cone hexagonal prism structure. And Mn-MIL-53(Fe)-0.3 had sharp edges and smooth surface structure. However, the particle size of the Mn-MIL-53(Fe)-0.3 was smaller than that of MIL-53(Fe).

The characteristic functional groups of obtained samples were revealed by FTIR spectroscopy measurement. As the FTIR spectra exhibited ([Fig. 2](#)), there were characteristic peaks occurred at the position of 3467, 1615, 1390, 750 and 538 cm<sup>-1</sup> in the MIL-53(Fe). The occurrence of the strong and wild peak at 3467 cm<sup>-1</sup> might be caused by the stretching vibration of the O—H, which might be the water molecules adsorbed on the surface of samples [[32](#)]. The stretching vibration of C=O might be the reason for the occurrence of the adsorption peak at 1615 cm<sup>-1</sup>. Besides, the strong peak at 1390 cm<sup>-1</sup> was corresponds to the symmetric vibrations of —COOH, which indicated that the presence of H<sub>2</sub>BDC as an organic ligand in the frameworks of the materials [[33](#)]. Furthermore, there was a bending vibration peak of C—H at the position of 750 cm<sup>-1</sup>, which was attributed to the benzene rings of the organic ligands [[34,35](#)]. Moreover, a adsorption peak was occurred at 538 cm<sup>-1</sup>, which was caused by the stretching vibration of Fe—O [[36](#)]. The characteristic peaks of Mn-doped MIL-53(Fe) appeared in the same position as that of MIL-53(Fe) which confirmed that they had the same structure [[37](#)]. The absence of distinct characteristic peaks of Mn—O might be due to its lower relative content than Fe.

The XRD pattern ([Fig. 3](#)) showed that the pristine MIL-53(Fe) had the characteristic peaks as reported in the literature which confirmed the synthesis of MIL-53(Fe) was successful [[38](#)]. Compared with the virgin MIL-53(Fe), the characteristic peaks of the five Mn-doped MOFs appeared in the same position but the intensity of the characteristic peaks changed. It indicated that the crystal structure of Mn-doped MIL-53(Fe) was the same as the original MIL-53(Fe). Thus, the analysis results of XRD were consistent with FTIR. The undetected peaks of manganese oxide and manganese salt might be caused by the partial isomorphism of Mn replacing Fe [[39](#)].

The N<sub>2</sub> adsorption and desorption isotherms of the synthesized samples were carried out to further explore their surface area, pore diameter and pore volume. The obtained parameters and pore size distributions (inserted) were demonstrated in [Fig. 4](#) and [Table 1](#). Obviously, it exhibited the typical type 1 curve, which might be attribute to its microporous structure. Moreover, the pore size dis-

tribution showed the existence of micropores which the pore diameter mainly concentrated at 0–20 nm. The surface area of MIL-53(Fe) and Mn-MIL-53(Fe)-0.3 were 231.63 and 405.95 m<sup>2</sup> g<sup>-1</sup>, respectively. The pore volume of MIL-53(Fe) was 0.135 cm<sup>3</sup> g<sup>-1</sup>. After doping Mn<sup>2+</sup>, the pore volume increased to 0.213 cm<sup>3</sup> g<sup>-1</sup>. The pore size distributions images (inserted) also showed that the pore size of the sample was mainly distributed in micropores [[40](#)].

#### 3.2. Catalytic performance of materials

The catalytic performance and kinetic behavior of Mn-MIL-53(Fe)/PMS systems for TC degradation were shown in [Fig. 5a](#). The results demonstrated that 43.1% degradation efficiency of TC was attained within 60 min in MIL-53(Fe)/PMS system, while the degradation efficiencies of TC were 89.8% and 93.2% in Mn-MIL-53(Fe)-0.5/PMS and Mn-MIL-53(Fe)-0.3/PMS systems, respectively. In addition, the degradation efficiency decreased to 76.6% in Mn-MIL-53(Fe)-3/PMS system and 83.5% in Mn-MIL-53(Fe)-2/PMS system. Moreover, the degradation efficiency of TC in the control experiment with only PMS was 26.1%. Correspondingly, [Fig. 5b](#) showed that *k*<sub>obs</sub> of TC removal increased from 0.0042 min<sup>-1</sup> (only PMS) to 0.0428 min<sup>-1</sup> (Mn-MIL-53(Fe)-0.3). And the *k*<sub>obs</sub> of MIL-53(Fe), Mn-MIL-53(Fe)-3, Mn-MIL-53(Fe)-2, Mn-MIL-53(Fe)-1 and Mn-MIL-53(Fe)-0.5 was calculated as 0.0128, 0.0265, 0.0308, 0.0331 and 0.0381 min<sup>-1</sup>, respectively. Therefore, the following studies were conducted by Mn-MIL-53(Fe)-0.3 to better elucidate the catalytic performance of Mn-MIL-53(Fe)/PMS systems.

#### 3.3. Effect of PMS dosage and catalyst dosage

The effect of PMS dosage and catalyst dosage was investigated. [Fig. 3\(a-b\)](#) demonstrated that the removal efficiency of TC and *k*<sub>obs</sub> improved continuously with the increasing concentrations of PMS from 0.1 g L<sup>-1</sup> to 0.3 g L<sup>-1</sup>. This might be due to the fact that an increase concentration of PMS caused the catalysts to generate more free radicals [[41](#)]. However, the removal efficiency of TC decreased to 89.1% when PMS concentrations increased to 0.4 g L<sup>-1</sup>. This phenomenon might be attributed to that the excessive PMS could quench free radicals [[42](#)]. Therefore, the following catalytic experiments were carried out under the condition of the PMS concentration at 0.3 g L<sup>-1</sup>.

As shown in [Fig. 6\(c-d\)](#), the catalytic performance was obviously improved by increasing the concentration of catalyst from 0.05 g L<sup>-1</sup> to 0.4 g L<sup>-1</sup>. The reaction constant *k*<sub>obs</sub> increased from 0.0187 min<sup>-1</sup> to 0.0464 min<sup>-1</sup>. Actually, a higher catalyst concentration could provide more active sites, which is conducive for the activation of PMS and promoted the degradation efficiency of TC. However, the TC removal curves showed that when the catalyst concentration increased from 0.2 g L<sup>-1</sup> to 0.4 g L<sup>-1</sup>, the degradation efficiency of TC was improved slightly. Based on the above experimental results, a catalyst dosage of 0.2 g L<sup>-1</sup> was determined for the further experimental.

#### 3.4. Effect of experimental conditions on catalytic activity of materials

The removal efficiency of TC by Mn-MIL-53(Fe)-0.3/PMS system was evaluated at different temperatures. As displayed in [Fig. S1a](#), 93.2% removal efficiency of TC was attained at 25 °C in Mn-MIL-53(Fe)-0.3/PMS system. With the temperature increased to 35 °C, 45 °C and 55 °C, the degradation efficiency of TC reached to 94.3%, 95.1% and 96.2%, respectively. And [Fig. S1b](#) showed that with the solution temperature increased, the kinetics constant (*k*<sub>obs</sub>, min<sup>-1</sup>) gradually increased. This might be attributed to that the increased temperature was conducive to the thermal activation

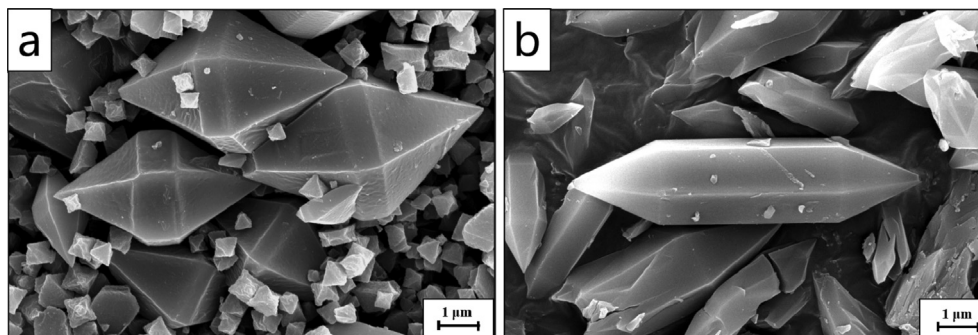


Fig. 1. The SEM images of MIL-53(Fe) (a) and Mn-MIL-53(Fe)-0.3 (b).

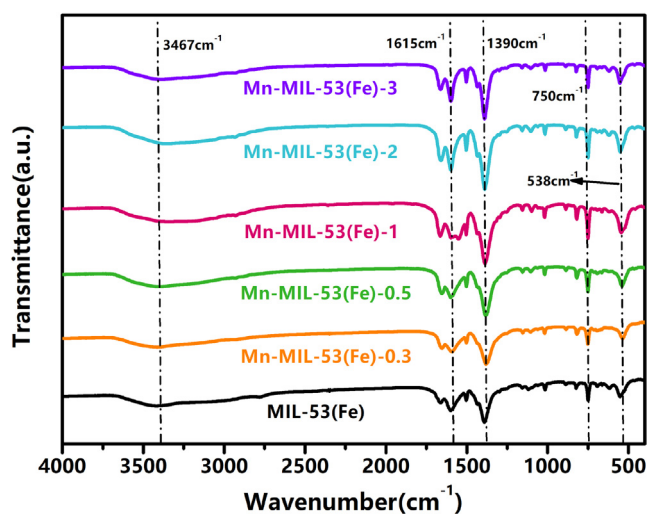


Fig. 2. The FTIR spectroscopy of the samples.

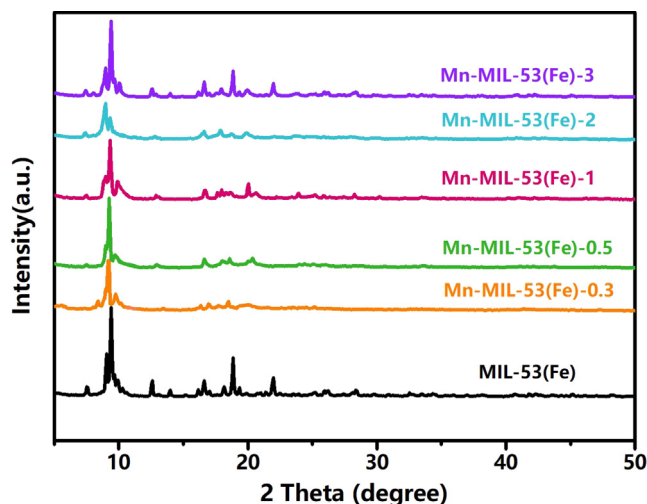


Fig. 3. The XRD patterns of the samples.

of PMS, which generated more active radicals to degrade TC [43]. Therefore, the increasing temperature was beneficial to the catalytic degradation of TC. What's more, the reaction activation energy ( $E_a$ ) could be obtained from Eq. (3).

$$\ln k_{\text{obs}} = \ln A - E_a/RT \quad (3)$$

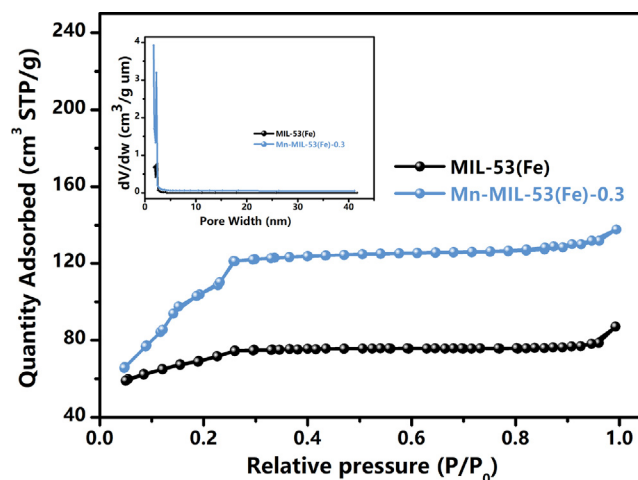


Fig. 4. N<sub>2</sub> adsorption-desorption isotherms and pore size distributions images (inserted) of MIL-53(Fe) and Mn-MIL-53(Fe)-0.3.

Table 1

Surface area, pore size and pore volume parameters of MIL-53(Fe) and Mn-MIL-53(Fe).

Samples	Surface area <sup>a</sup> (m <sup>2</sup> g <sup>-1</sup> )	Pore size <sup>b</sup> (nm)	Pore volume <sup>c</sup> (cm <sup>3</sup> g <sup>-1</sup> )
MIL-53(Fe)	231.63	2.717	0.135
Mn-MIL-53(Fe)-0.3	405.95	2.265	0.213

<sup>a</sup> Measured using N<sub>2</sub> adsorption with the Brunauer-Emmett-Teller (BET) method.

<sup>b</sup> Pore size in diameter calculated by the desorption data using Barrett-Joyner-Halenda (BJH) method.

<sup>c</sup> Total pore volume determined at P/P<sub>0</sub> = 0.99.

In Eq. (3),  $k_{\text{obs}}$  (min<sup>-1</sup>) is the overall pseudo-first-order rate constant which could be calculated by equation (S1) in the Supporting Information, A is constant, R (8.314 J mol<sup>-1</sup> K<sup>-1</sup>) is the gas constant,  $E_a$  (KJ mol<sup>-1</sup>) is the reaction activation energy and T (K) is thermodynamic temperature.

The thermodynamic fitting curve can be seen in Fig. S2. According to the slope of the fitting curve, the value of  $E_a$  was calculated as 4.629 kJ mol<sup>-1</sup>, which indicated that the TC removal in Mn-MIL-53(Fe)/PMS system was an endothermic reaction.

The catalytic performance of Mn-MIL-53(Fe) under the condition of different initial pH values were evaluated. The results indicated that when the initial pH values varied from 2.0 to 12.0, the removal efficiency of TC increased continuously. As Fig. 7 showed, the degradation efficiency of TC with pH of 4.0–12.0 was up to more than 84% within 60 min, while only 70% of TC was degraded

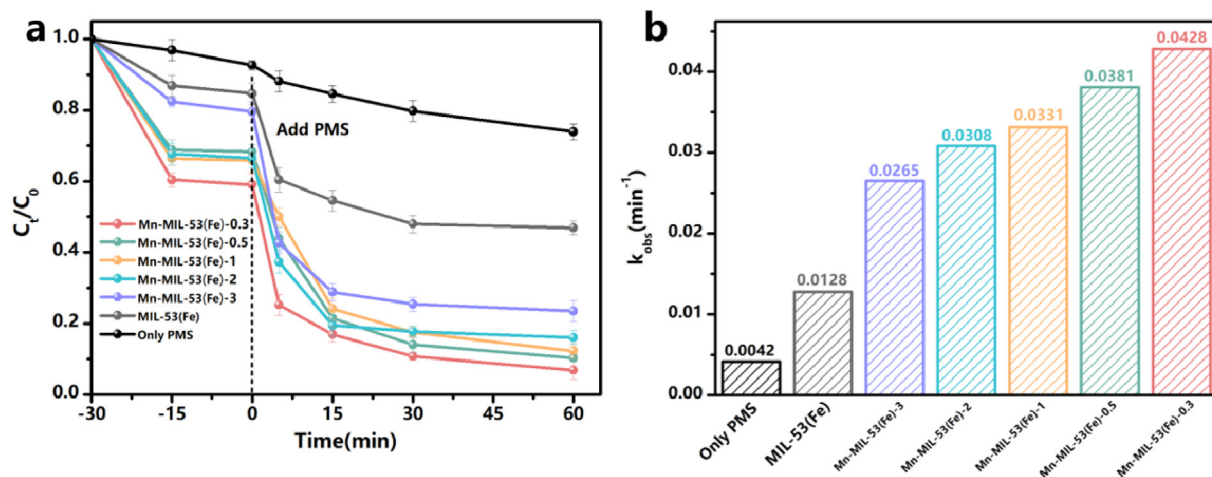


**Fig. 5.** The degradation efficiency (a) and kinetics constant (b) of TC in the Mn-MIL-53(Fe)/PMS system. Experimental conditions: catalyst dosage = 0.2 g L<sup>-1</sup>; initial TC concentration = 30 mg L<sup>-1</sup>; PMS concentration = 0.3 g L<sup>-1</sup>.

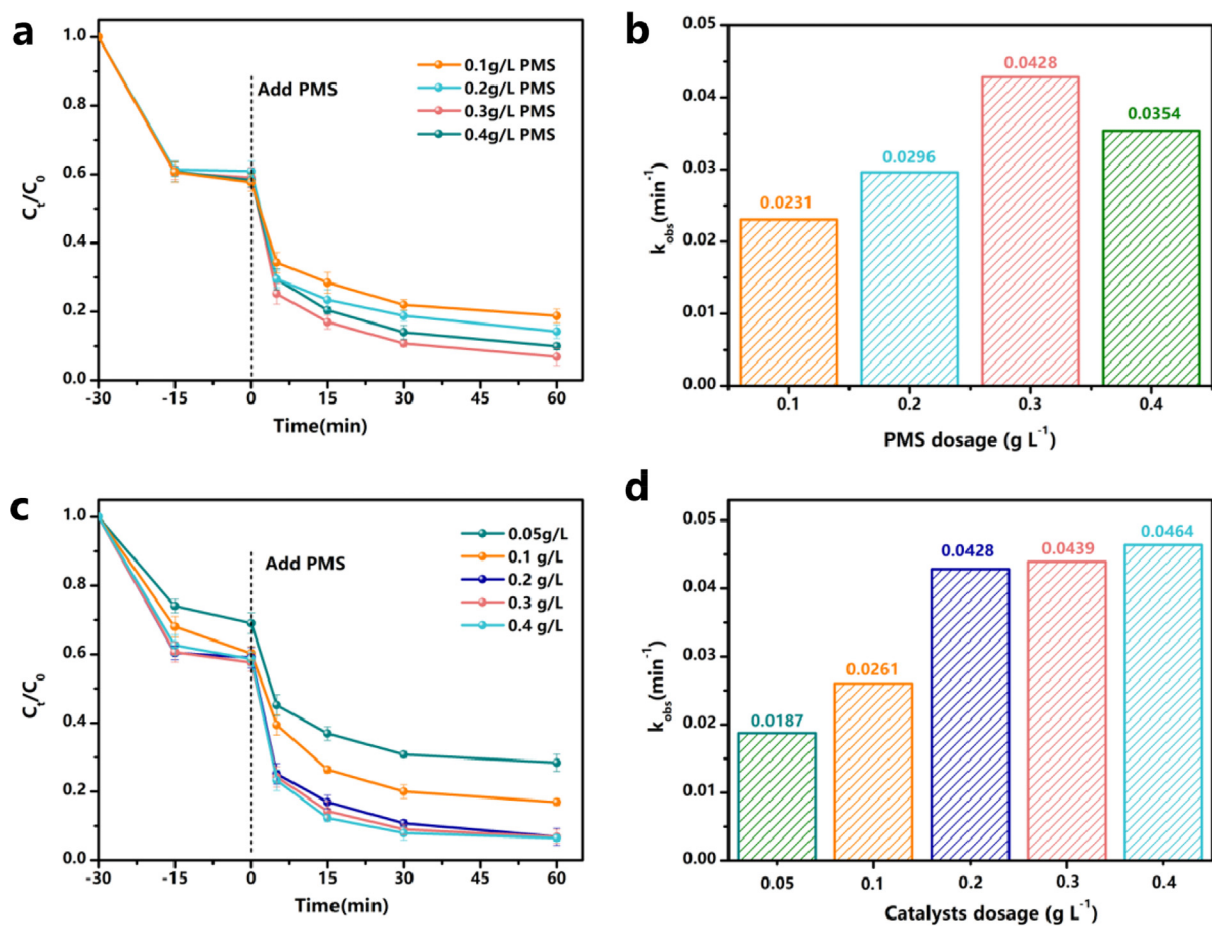


**Fig. 6.** Effects for the catalytic degradation of TC by Mn-MIL-53(Fe)/PMS system: (a, b) effect of oxidant dosage and kinetics constant; (c, d) effect of catalysts dosage and kinetics constant. Experimental conditions: catalyst dosage = 0.2 g L<sup>-1</sup> (0.05, 0.1, 0.2, 0.3, 0.4 g L<sup>-1</sup> in Fig. 6c); initial TC concentration = 30 mg L<sup>-1</sup>; PMS concentration = 0.3 g L<sup>-1</sup> (0.1, 0.2, 0.3, 0.4, g L<sup>-1</sup> in Fig. 6a).

in extremely acidity condition of pH = 2.0. As the initial pH values increased from 2.0 to 12.0, the removal efficiency of TC increased obviously. The results illustrated that Mn-MIL-53(Fe)/PMS system with initial pH values between 4.0 and 12.0 was more beneficial to the degrade of TC compared with pH = 2.0. This phenomenon could be attributed that HSO<sub>5</sub><sup>-</sup> was vulnerable by catalytic attack under

alkaline conditions [44]. In addition, the lowest removal efficiency of TC at pH = 2.0 might due to there was a passivation phenomenon occur on Mn-MIL-53(Fe)-0.3 under extremely acidity condition [45].

Inorganic ions and humic acids were abundant in natural waters, it is important to explore their effects on TC removal in

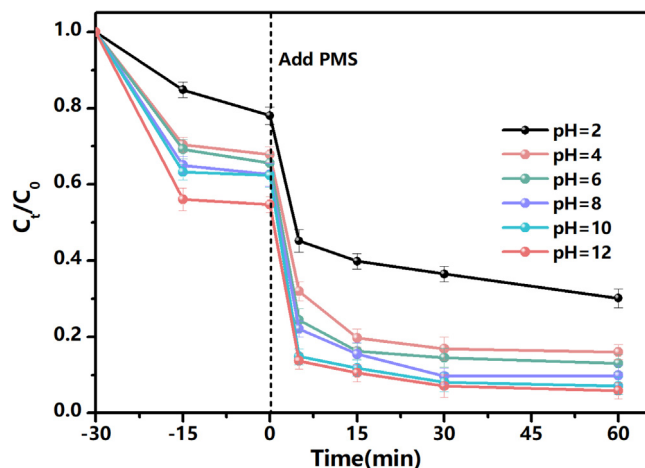


**Fig. 7.** The effect of initial pH on TC degradation efficiency. Experimental conditions: catalyst dosage =  $0.2 \text{ g L}^{-1}$ ; initial TC concentration =  $30 \text{ mg L}^{-1}$ ; PMS concentration =  $0.3 \text{ g L}^{-1}$ .

Mn-MIL-53(Fe)/PMS systems. Thus, the effects of the concentration of coexisting anions ( $\text{Cl}^-$ ,  $\text{CO}_3^{2-}$  and  $\text{SO}_4^{2-}$ ) and HA on the removal efficiency of TC in the Mn-MIL-53(Fe)/PMS system were investigated. As shown in Fig. S3a, the TC degradation efficiency decreased from 93.2% to 82.8% due to the increased of the concentration of  $\text{Cl}^-$ . This phenomenon might be due to that  $\text{Cl}^-$  could react with  $\text{SO}_4^-$  and  $\text{HO}^-$ , which caused the concentration of free radicals involved in TC degradation decreased [46]. And Fig. S3b indicated that the presence of  $\text{CO}_3^{2-}$  resulting in the decrease of the TC removal efficiency. It might be attributed to that  $\text{CO}_3^{2-}$  could react with free radicals to produce  $\text{SO}_3^-$  with weaker activity [47]. In addition, the  $\text{SO}_3^-$  might directly react with  $\text{HSO}_5^-$  to generated  $\text{HCO}_4^-$  [48,49]. Fig. S3c showed that the  $\text{SO}_4^{2-}$  in solution had slightly effect on the removal of TC. Moreover, Fig. S3d suggested that the addition of HA in solution could inhibited the degradation efficiency of TC in the Mn-MIL-53(Fe)/PMS systems. With the increased of HA concentrations, the degradation efficiency of TC decreased from 88.9% to 86.1%. The reason for this phenomenon might be that the HA molecules could react with free radicals, forming a competitive relationship with the TC molecules in solution. Additionally, the HA molecules might interact with the catalyst through  $\pi$ - $\pi$  interactions, resulting in a decrease of active sites [50,51]. Overall, the effects of inorganic ions and HA on materials activation of PMS for TC degradation should be considered adequately.

To test the practicability of the Mn-MIL-53(Fe)/PMS systems, the degradation efficiency of TC in tap water, river water and medical water (water related parameters were given in Table 2) was further evaluated in Fig. 8. The Mn-MIL-53(Fe)/PMS systems had the highest TC removal efficiency in ultrapure water. The degradation efficiency of TC in tap water and river water were 82.1% and 84.4%, respectively. However, the efficiency of removing TC from medical water was lowest, only 74%. This phenomenon might be caused by the presence of organic compounds or pollutants in actual water could react with active radicals, which slightly limiting the degradation of TC in solution. Overall, Mn-MIL-53(Fe)/PMS systems had good TC removal efficiency in actual water [52].

### 3.5. Mechanism discussion

The XPS analysis was performed to characterized the samples of MIL-53(Fe) and Mn-MIL-53(Fe)-0.3 before and after reaction. As displayed in Fig. 9a, the XPS survey spectrum of MIL-53(Fe) con-

**Table 2**  
The quality parameters of tap water, river water and medical wastewater.

Water type	pH	COD ( $\text{mg L}^{-1}$ )	TOC ( $\text{mg L}^{-1}$ )
Tap water	7.54	1.832	0.625
River water	7.62	48.73	21.39
Medical water	6.65	25,300	5149.38

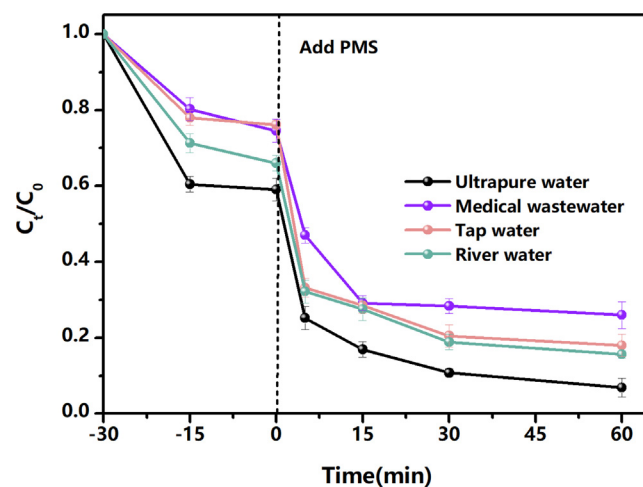


**Fig. 8.** Removal efficiency of TC by Mn-MIL-53(Fe)-0.3 in real samples. Experimental conditions: catalyst dosage =  $0.2 \text{ g L}^{-1}$ ; initial TC concentration =  $30 \text{ mg L}^{-1}$ ; PMS concentration =  $0.3 \text{ g L}^{-1}$ .

tains Fe, C and O, and the XPS survey spectrum of Mn-MIL-53(Fe)-0.3 indicated the existence of Mn, Fe, C and O. It could be seen from the Fe2p spectrum of the Mn-MIL-53(Fe)-0.3 (Fig. 9b), the binding energy at 710.35 eV correspond to the Fe(II) and the binding energy at 715.19 eV ascribed to satellite peak [53]. In addition, the relative content of Fe(II) before reaction was 35.61% and increased to 48.31% after reaction. This indicated that Fe(II) and Fe(III) in the catalysts were involved in the catalytic reaction. The XPS spectrum of Mn2p was showed in Fig. 9c, the  $\text{Mn}2p_{3/2}$  peak could be divided into three peaks at 639.9 eV, 641.1 eV and 645.2 eV, which matched with Mn(II), Mn(III) and the satellite peak, respectively [54]. More importantly, the relative content of Mn(II) before reaction was 13.12% and increased to 29.54% after reaction. It can also be seen that the relative contents of Mn(III) were 42.29% before reaction and changed to 27.63% after reaction. It indicated that the valence state of Mn changes obviously in the catalytic process.

It is well known that the radicals generated by the catalyst activation of PMS were  $\text{SO}_4^-$  and  $\text{HO}^-$  [55]. The radical scavenging experiments were carried out to confirm the main active radicals involving in the catalytic reactions. The radicals in the Mn-MIL-53(Fe)/PMS systems were trapped by Methanol (MeOH) and *tert*-butanol (TBA). MeOH is the scavenger for both  $\text{SO}_4^-$  and  $\text{HO}^-$  radicals, while TBA is the scavenger for  $\text{HO}^-$  rather than  $\text{SO}_4^-$  [56]. The results shown in Fig. 10a illustrated that both TBA and MeOH could inhibited the TC degradation but the magnitude of the effect was varied. The trapping agent of TBA reduced the removal efficiency of TC slightly, from 93.2% to 86.7%, while after the addition of MeOH, the removal efficiency decreased to 70.6%. This phenomenon suggested that MeOH had a strong inhibitory effect on the reaction, which also indicated that both  $\text{SO}_4^-$  and  $\text{HO}^-$  were involved in the reaction, and  $\text{SO}_4^-$  was more dominant compared with  $\text{HO}^-$ . The types and intensities of radicals produced at different time in the Mn-MIL-53(Fe)/PMS system were determined by EPR characterization. And the results displayed in Fig. 10b, it was

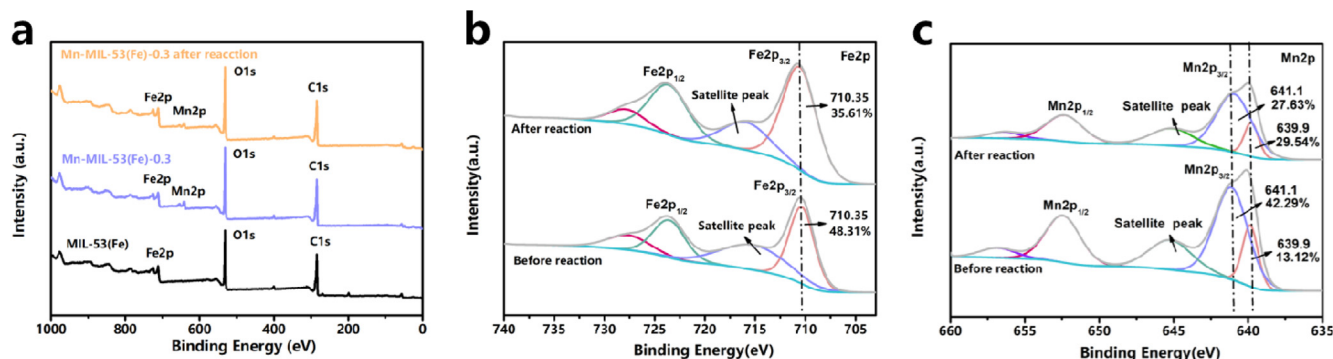


**Fig. 9.** The XPS spectrum of MIL-53(Fe) and Mn-MIL-53(Fe)-0.3 before and after reaction (a), Fe2p XPS spectra (b) and Mn2p XPS spectra (c) of Mn-MIL-53(Fe)-0.3 before and after reaction. Experimental conditions: catalyst dosage = 0.2 g L<sup>-1</sup>; initial TC concentration = 30 mg L<sup>-1</sup>; PMS concentration = 0.3 g L<sup>-1</sup>.

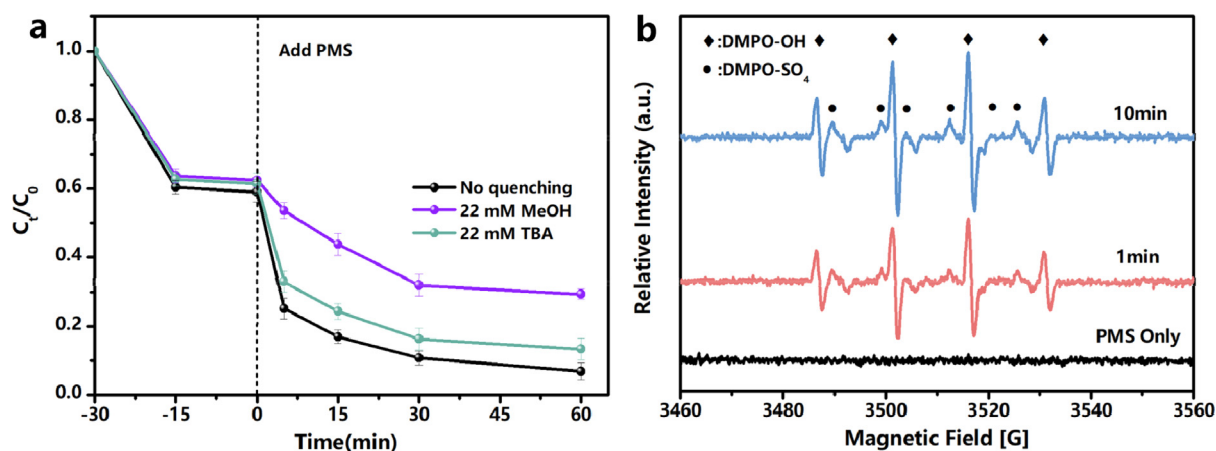
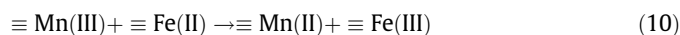
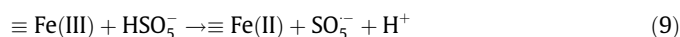
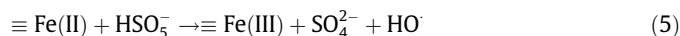


**Fig. 10.** Effect of different radical quenchers on TC degradation in Mn-MIL-53(Fe)/PMS system (a) and EPR spectra obtained by using DMPO as spin-trapping agent (b). Experimental conditions: catalyst dosage = 0.2 g L<sup>-1</sup>; initial TC concentration = 30 mg L<sup>-1</sup>; PMS concentration = 0.3 g L<sup>-1</sup>.

obviously that the characteristic signals of DMPO-OH and DMPO-SO<sub>4</sub> could be detected, which could verify the results of the radical scavenging experiment. In addition, the intensity of the two characteristic signals enhanced when the time increased from 1 min to 10 min, indicating that Mn-MIL-53(Fe) activated PMS to generate more SO<sub>4</sub><sup>-</sup> and HO<sup>-</sup> involved in the catalytic reaction. Therefore, both SO<sub>4</sub><sup>-</sup> and HO<sup>-</sup> played a leading role in the Mn-MIL-53(Fe)/PMS system towards the TC degradation.

According to the previous BET analysis, Mn-MIL-53(Fe)-0.3 had a larger specific surface area (405.95 m<sup>2</sup> g<sup>-1</sup>), which was conducive to adsorb TC molecules for contact with the active site. Besides, a larger specific surface area could provide more active sites for the activation of PMS, thus improving its catalytic performance [57]. FTIR spectroscopy showed that the strong and wild peak at 3467 cm<sup>-1</sup> was caused by the stretching vibration of water-bonded O–H. Moreover, the adsorption peak occurred at 538 cm<sup>-1</sup>, which was caused by the stretching vibration of Fe–O and Mn–O. This indicated that there might be a hydroxylation reaction during surface activation [58]. Based on the above analysis results, the possible mechanism of Mn-MIL-53(Fe) activating PMS to generate radicals was described as follows. At first, the sites of Fe(II) and Mn(II) on the catalysts generated SO<sub>4</sub><sup>-</sup> and HO<sup>-</sup> by providing electrons to activated PMS, Fe(II) and Mn(II) also transform into Mn(III) and Fe(III) after losing electrons (Eqs. (4)–(7)). Subsequently, the Mn(III) and Fe(III) sites obtaining electrons to activated PMS, the SO<sub>4</sub><sup>-</sup> radicals and the sites of Mn(II) and Fe(II) were generated, which forming a cycle of Mn and Fe (Eqs. (8)–(10)) [59–61]. Finally, the generated SO<sub>4</sub><sup>-</sup> and HO<sup>-</sup> radicals could

be applied to degrade TC molecules efficiently. The catalytic performance of Mn-MIL-53(Fe) was superior to MIL-53(Fe), which might be due to the synergistic effect could occurred between Mn and Fe [62]. Furthermore, the rate of electron transfer could be enhanced due to the redox reaction occurred between Mn and Fe, which improved the activity of SO<sub>4</sub><sup>-</sup> and HO<sup>-</sup> produced by PMS, and both improved the degradation efficiency and reusability of catalysts. The possible mechanism was showed in Fig. 11.



### 3.6. Degradation pathways

The TC degradation intermediates were measured by LC-MS techniques and the mass spectrometry was used to speculated

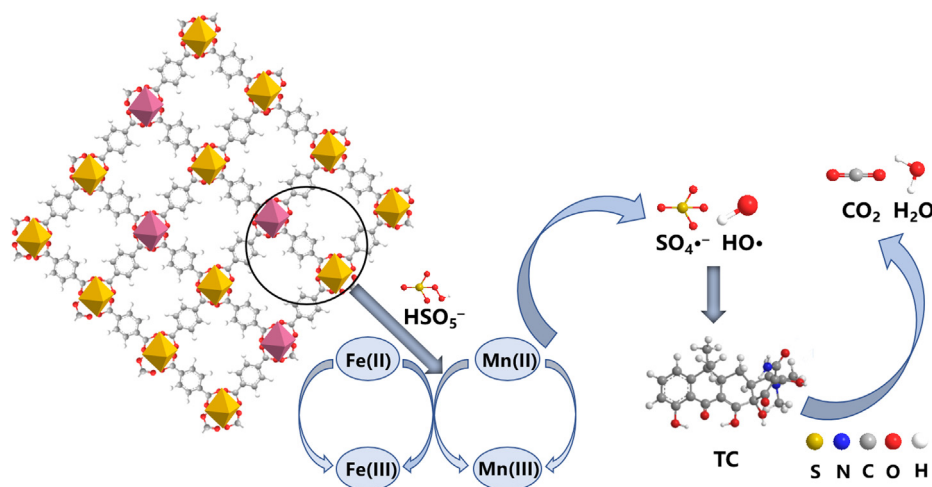


Fig. 11. Possible reaction mechanism of TC degradation by Mn-MIL-53(Fe)/PMS system.

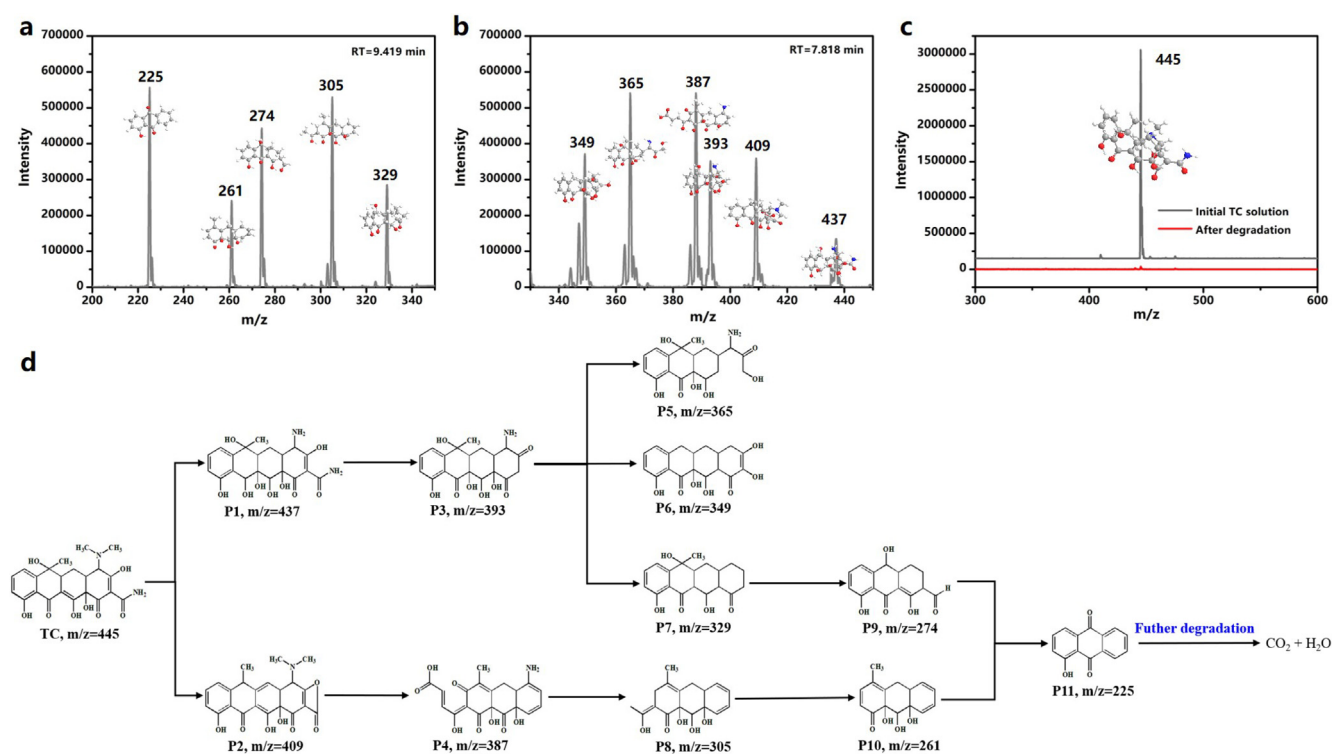


Fig. 12. LC-MS analysis of TC intermediates in the degradation reaction with Mn-MIL-53(Fe) (a–b); LC-MS analysis of TC before and after TC degradation (c); the proposed transformation pathways of TC degradation (d).

the possible structures of the intermediates. The detected intermediates and their possible molecular structures contained P1( $m/z = 437$ ), P2( $m/z = 409$ ), P3( $m/z = 393$ ), P4( $m/z = 387$ ), P5( $m/z = 365$ ), P6( $m/z = 349$ ), P7( $m/z = 329$ ), P8( $m/z = 305$ ), P9( $m/z = 274$ ), P10( $m/z = 261$ ) and P11( $m/z = 225$ ), were shown in Fig. 12a and Fig. 12b. In addition, Fig. 12c showed that the concentration of TC before and after the reaction had a great change and decreased a lot. According to the identification of the intermediate, the potential degradation pathway of TC was analyzed. As presented in Fig. 12d, the TC degradation pathways including hydroxylation, dealkylation, and dehydration. Briefly, the TC molecular with  $m/z = 445$  was firstly reacted with  $\text{SO}_4^{\bullet-}$  and  $\text{HO}^{\bullet}$  to generated its dealkylation product ( $m/z = 437$ ) and dehydration product ( $m/z = 409$ ). After that, it was transformed into low molecular weight

products through a series of reactions and finally oxidized into  $\text{CO}_2$  and  $\text{H}_2\text{O}$  [63,64]. Besides, according to the results of total organic carbon (TOC) analyzer, the removal efficiency of TC by Mn-MIL-53(Fe)/PMS system was 50.6%.

### 3.7. Reusability of Mn-MIL-53(Fe) catalyst and stability tests

A catalyst with good performance should be recyclable, so it is important to separate the used catalyst from the bulk solution. In this experiment, the catalysts were washed several times by ethanol after centrifugation, and then the cycle experiment was carried out after drying. Based on this, the reusability of the Mn-MIL-53(Fe)/PMS was showed in Fig. S4. Obviously, the TC degradation efficiency in the Mn-MIL-53(Fe)/PMS systems decreased from 93.2% to

82.6% and 80.6% after third and fourth cycles. Thus, the Mn-MIL-53(Fe)/PMS system still had good reusability after several cycle tests. Furthermore, the leaching experiments of Mn and Fe during the reaction process were measured by ICP-MS to evaluate the stability of MIL-53(Fe)/PMS system. As showed in Fig. S5, the maximum leaching concentration of Mn and Fe during the reaction process were  $0.66 \text{ mg L}^{-1}$  and  $0.37 \text{ mg L}^{-1}$ , respectively. This leaching concentration of Mn and Fe were not sufficient to activate PMS, which indicated that MIL-53(Fe) activates PMS was a heterogeneous process [49]. And the leaching concentration of Mn and Fe were low, indicating that the MIL-53(Fe)/PMS system was stable.

#### 4. Conclusion

In summary, the Mn-doped MIL-53(Fe) catalysts were synthesized via a facile solvothermal process and exhibited excellent PMS activation performance to eliminate TC from aqueous solutions. The removal efficiency of TC was achieved 93.2% within 60 min in the Mn-MIL-53(Fe)-0.3/PMS system, and the observed  $k_{\text{obs}}$  was  $0.0428 \text{ min}^{-1}$ , which was 3.34 times than that of the pristine MIL-53(Fe). The change of TC degradation efficiency at different temperatures indicated that the TC degradation is an endothermic process. In addition, the degradation of TC in Mn-MIL-53(Fe)/PMS systems were obviously affected under different conditions of initial pH, co-existing ions and humic acid. More importantly, the main reactive radicals in TC degradation process were  $\text{SO}_4^-$  and  $\text{HO}^-$  free radicals, which was confirmed by the experiments of radical scavengers and EPR. Furthermore, the XPS characterization results explained that the active radicals of  $\text{SO}_4^-$  and  $\text{HO}^-$  were generated by the Fe(II) and Mn(II) active sites on the catalyst surface. Besides, the TC degradation intermediates were obtained by LC-MS and possible degradation pathways were proposed including hydroxylation, dealkylation, and dehydration process. Moreover, the catalysts also showed good performance in actual water treatment and had good recoverability. Therefore, this study provided a feasible method for the preparation of MOFs-based catalysts to eliminate the antibiotic pollutants in wastewater.

#### Declaration of Competing Interest

The authors declare that they have no known competing financial interests or personal relationships that could have appeared to influence the work reported in this paper.

#### Acknowledgement

The study was financially supported by the National Natural Science Foundation of China (51878258, 51521006 and 41807125).

#### Appendix A. Supplementary data

Supplementary data to this article can be found online at <https://doi.org/10.1016/j.jcis.2020.07.045>.

#### References

- [1] A.K. Sarmah, M.T. Meyer, A.B.A. Boxall, A global perspective on the use, sales, exposure pathways, occurrence, fate and effects of veterinary antibiotics (VAs) in the environment, *Chemosphere* 65 (5) (2006) 725–759.
- [2] N. Pastor-Navarro, A. Maquieira, R. Puchades, Review on immunoanalytical determination of tetracycline and sulfonamide residues in edible products, *Anal. Bioanal. Chem.* 395 (4) (2009) 907–920.
- [3] R. Xu, Z.-H. Yang, Y. Zheng, Q.-P. Wang, Y. Bai, J.-B. Liu, Y.-R. Zhang, W.-P. Xiong, Y. Lu, C.-Z. Fan, Metagenomic analysis reveals the effects of long-term antibiotic pressure on sludge anaerobic digestion and antimicrobial resistance risk, *Bioresour. Technol.* 282 (2019) 179–188.
- [4] P. Song, Z. Yang, H. Xu, J. Huang, X. Yang, F. Yue, L. Wang, Arsenic removal from contaminated drinking water by electrocoagulation using hybrid Fe-Al electrodes: response surface methodology and mechanism study, *Desalin. Water Treat.* 57 (10) (2016) 4548–4556.
- [5] P. Song, Q. Song, Z. Yang, G. Zeng, H. Xu, X. Li, W. Xiong, Numerical simulation and exploration of electrocoagulation process for arsenic and antimony removal: Electric field, flow field, and mass transfer studies, *J. Environ. Manage.* 228 (2018) 336–345.
- [6] R. Xu, Z.-H. Yang, Y. Zheng, H.-B. Zhang, J.-B. Liu, W.-P. Xiong, Y.-R. Zhang, K. Ahmad, Depth-resolved microbial community analyses in the anaerobic co-digester of dewatered sewage sludge with food waste, *Bioresour. Technol.* 244 (2017) 824–835.
- [7] Y. Bai, R. Xu, Q.-P. Wang, Y.-R. Zhang, Z.-H. Yang, Sludge anaerobic digestion with high concentrations of tetracyclines and sulfonamides: Dynamics of microbial communities and change of antibiotic resistance genes, *Bioresour. Technol.* 276 (2019) 51–59.
- [8] M. Jia, Z. Yang, H. Xu, P. Song, W. Xiong, J. Cao, Y. Zhang, Y. Xiang, J. Hu, C. Zhou, Y. Yang, W. Wang, Integrating N and F co-doped TiO<sub>2</sub> nanotubes with ZIF-8 as photoelectrode for enhanced photo-electrocatalytic degradation of sulfamethazine, *Chem. Eng. J.* 388 (2020) 124388.
- [9] Y. Deng, Z. Li, R. Tang, K. Ouyang, C. Liao, Y. Fang, C. Ding, L. Yang, L. Su, D. Gong, What will happen when microorganisms “meet” photocatalysts and photocatalysis?, *Environ. Sci.-Nano* 7 (3) (2020) 702–723.
- [10] Y. Deng, C. Feng, L. Tang, Y. Zhou, Z. Chen, H. Feng, J. Wang, J. Yu, Y. Liu, Ultrathin low dimensional heterostructure composites with superior photocatalytic activity: insight into the multichannel charge transfer mechanism, *Chem. Eng. J.* 393 (2020) 124718.
- [11] Y. Li, L. Pan, Y. Zhu, Y. Yu, D. Wang, G. Yang, X. Yuan, X. Liu, H. Li, J. Zhang, How does zero valent iron activating peroxydisulfate improve the dewatering of anaerobically digested sludge?, *Water Res.* 163 (2019).
- [12] P. Hu, M. Long, Cobalt-catalyzed sulfate radical-based advanced oxidation: a review on heterogeneous catalysts and applications, *Appl. Catal. B-Environ.* 181 (2016) 103–117.
- [13] G. Wei, X. Liang, Z. He, Y. Liao, Z. Xie, P. Liu, S. Ji, H. He, D. Li, J. Zhang, Heterogeneous activation of Oxone by substituted magnetites Fe<sub>3-x</sub>MxO<sub>4</sub> (Cr, Mn, Co, Ni) for degradation of Acid Orange II at neutral pH, *J. Molecular Catal. A-Chemical* 398 (2015) 86–94.
- [14] E. Saputra, S. Muhammad, H. Sun, H.M. Ang, M.O. Tade, S. Wang, A comparative study of spinel structured Mn<sub>3</sub>O<sub>4</sub>, Co<sub>3</sub>O<sub>4</sub> and Fe<sub>3</sub>O<sub>4</sub> nanoparticles in catalytic oxidation of phenolic contaminants in aqueous solutions, *J. Colloid Interface Sci.* 407 (10) (2013) 467–473.
- [15] S.K. Ling, S. Wang, Y. Peng, Oxidative degradation of dyes in water using Co<sub>2</sub>/H<sub>2</sub>O<sub>2</sub> and Co<sub>2</sub>/peroxymonosulfate, *J. Hazard. Mater.* 178 (1–3) (2010) 385–389.
- [16] P. Shukla, H. Sun, S. Wang, H.M. Ang, M.O. Tade, Nanosized Co<sub>3</sub>O<sub>4</sub>/SiO<sub>2</sub> for heterogeneous oxidation of phenolic contaminants in waste water, *Separ. Purif. Technol.* 77 (2) (2011) 230–236.
- [17] E. Saputra, S. Muhammad, H. Sun, H.-M. Ang, M.O. Tade, S. Wang, A comparative study of spinel structured Mn<sub>3</sub>O<sub>4</sub>, Co<sub>3</sub>O<sub>4</sub> and Fe<sub>3</sub>O<sub>4</sub> nanoparticles in catalytic oxidation of phenolic contaminants in aqueous solutions, *J. Colloid Interface Sci.* 407 (2013) 467–473.
- [18] C. Tan, N. Gao, D. Fu, J. Deng, L. Deng, Efficient degradation of paracetamol with nanoscaled magnetic CoFe<sub>2</sub>O<sub>4</sub> and MnFe<sub>2</sub>O<sub>4</sub> as a heterogeneous catalyst of peroxymonosulfate, *Sep. Purif. Technol.* 175 (2017) 47–57.
- [19] H. Liang, H. Sun, A. Patel, P. Shukla, Z.H. Zhu, S. Wang, Excellent performance of mesoporous Co<sub>3</sub>O<sub>4</sub>/MnO<sub>2</sub> nanoparticles in heterogeneous activation of peroxymonosulfate for phenol degradation in aqueous solutions, *Appl. Catal. B-Environ.* 127 (2012) 330–335.
- [20] B. Yang, Z. Tian, B. Wang, Z. Sun, L. Zhang, Y. Guo, H. Li, S. Yan, Facile synthesis of Fe<sub>3</sub>O<sub>4</sub>/hierarchical-Mn<sub>3</sub>O<sub>4</sub>/graphene oxide as a synergistic catalyst for activation of peroxymonosulfate for degradation of organic pollutants, *RSC Adv.* 5 (27) (2015) 20674–20683.
- [21] E.M. Dias, C. Petit, Towards the use of metal-organic frameworks for water reuse: a review of the recent advances in the field of organic pollutants removal and degradation and the next steps in the field, *J. Mater. Chem. A* 4 (9) (2016) 3565–3566.
- [22] W. Xiong, Z. Zeng, X. Li, G. Zeng, R. Xiao, Z. Yang, H. Xu, H. Chen, J. Cao, C. Zhou, L. Qin, Ni-doped MIL-53(Fe) nanoparticles for optimized doxycycline removal by using response surface methodology from aqueous solution, *Chemosphere* 232 (2019) 186–194.
- [23] Z. Hasan, S.H. Jung, Removal of hazardous organics from water using metal-organic frameworks (MOFs): Plausible mechanisms for selective adsorptions, *J. Hazard. Mater.* 283 (2015) 329–339.
- [24] J. Cao, Z. Yang, W. Xiong, Y. Zhou, Y. Wu, M. Jia, S. Sun, C. Zhou, Y. Zhang, R. Zhong, Peroxymonosulfate activation of magnetic Co nanoparticles relative to an N-doped porous carbon under confinement: Boosting stability and performance, *Sep. Purif. Technol.* 250 (2020) 117237.
- [25] X. Li, J. Wan, Y. Wang, Z. Yan, H. Chi, S. Ding, Mechanism of accurate recognition and catalysis of diethyl phthalate (DEP) in wastewater by novel MIL100 molecularly imprinted materials, *Appl. Catal. B* 266 (2020) 118591.
- [26] X. Liao, F. Wang, F. Wang, Y. Cai, Y. Yao, B.-T. Teng, Q. Hao, L. Shuxiang, Synthesis of (100) surface oriented MIL-88A-Fe with rod-like structure and its enhanced fenton-like performance for phenol removal, *Appl. Catal. B* 259 (2019) 118064.
- [27] J. Cao, Z.-H. Yang, W.-P. Xiong, Y.-Y. Zhou, Y.-R. Peng, X. Li, C.-Y. Zhou, R. Xu, Y.-R. Zhang, One-step synthesis of Co-doped UiO-66 nanoparticle with enhanced

- removal efficiency of tetracycline: Simultaneous adsorption and photocatalysis, *Chem. Eng. J.* 353 (2018) 126–137.
- [28] C. Wang, X. Liu, N.K. Demir, J.P. Chen, K. Li, Applications of water stable metal-organic frameworks, *Chem. Soc. Rev.* 45 (18) (2016) 5107–5134.
- [29] A.H. Corma, H. García, F.X.L.I. Xamena, ChemInform abstract: engineering metal organic frameworks for heterogeneous catalysis, *Chem. Rev.* 110 (8) (2010) 4606–4655.
- [30] Z.-H. Yang, J. Cao, Y.-P. Chen, X. Li, W.-P. Xiong, Y.-Y. Zhou, C.-Y. Zhou, R. Xu, Y.-R. Zhang, Mn-doped zirconium metal-organic framework as an effective adsorbent for removal of tetracycline and Cr(VI) from aqueous solution, *Microporous Mesoporous Mater.* 277 (2019) 277–285.
- [31] L. Xie, Z. Yang, W. Xiong, Y. Zhou, J. Cao, Y. Peng, X. Li, C. Zhou, R. Xu, Y. Zhang, Construction of MIL-53(Fe) metal-organic framework modified by silver phosphate nanoparticles as a novel Z-scheme photocatalyst: Visible-light photocatalytic performance and mechanism investigation, *Appl. Surf. Sci.* 465 (2019) 103–115.
- [32] H. Lu, Z. Zhu, H. Zhang, J. Zhu, Y. Qiu, Simultaneous removal of arsenate and antimonate in simulated and practical water samples by adsorption onto Zn/Fe layered double hydroxide, *Chem. Eng. J.* 276 (2015) 365–375.
- [33] C. Zhang, L. Ai, J. Jing, Graphene hybridized photoactive iron terephthalate with enhanced photocatalytic activity for the degradation of rhodamine B under visible light, *Ind. Eng. Chem. Res.* 54 (1) (2015) 153–163.
- [34] A. Banerjee, R. Gokhale, S. Bhatnagar, J. Jog, M. Bhardwaj, B. Lefez, B. Hannyer, S. Ogale, MOF derived porous carbon-Fe<sub>3</sub>O<sub>4</sub> nanocomposite as a high performance, recyclable environmental superadsorbent, *J. Mater. Chem.* 22 (37) (2012) 19694–19699.
- [35] P. Horcajada, C. Serre, G. Maurin, N.A. Ramsahye, F. Balas, M. Vallet-Regi, M. Sebban, F. Taulelle, G. Férey, Flexible porous metal-organic frameworks for a controlled drug delivery, *J. Am. Chem. Soc.* 130 (21) (2008) 6774–6780.
- [36] J. Yu, W. Xiong, X. Li, Z. Yang, J. Cao, M. Jia, R. Xu, Y. Zhang, Functionalized MIL-53(Fe) as efficient adsorbents for removal of tetracycline antibiotics from aqueous solution, *Microporous Mesoporous Mater.* 290 (2019).
- [37] H. Li, W. Shi, K. Zhao, H. Li, Y. Bing, P. Cheng, Enhanced hydrostability in Ni-doped MOF-5, *Inorg. Chem.* 51 (17) (2012) 9200–9207.
- [38] M.I. Breeze, G. Clet, B.C. Campo, A. Vimont, M. Daturi, J.-M. Grenèche, A.J. Dent, F. Millange, R.I. Walton, Isomorphous substitution in a flexible metal-organic framework: mixed-metal, mixed-valent MIL-53 type materials, *Inorg. Chem.* 52 (14) (2013) 8171–8182.
- [39] G. Zhou, M.F. Wu, Q.J. Xing, F. Li, H. Liu, X.B. Luo, J.P. Zou, J.M. Luo, A.Q. Zhang, Synthesis and characterizations of metal-free Semiconductor/MOFs with good stability and high photocatalytic activity for H<sub>2</sub> evolution: a novel Z-Scheme heterostructured photocatalyst formed by covalent bonds, *Appl. Catal. B-Environ.* 220 (2018) 607–614.
- [40] M. Pu, Z. Guan, Y. Ma, J. Wan, Y. Wang, M.L. Brusseau, H. Chi, Synthesis of iron-based metal-organic framework MIL-53 as an efficient catalyst to activate persulfate for the degradation of Orange G in aqueous solution, *Applied Catalysis a-General* 549 (2018) 82–92.
- [41] P. Shukla, H. Sun, S. Wang, H.M. Ang, M.O. Tade, Co-SBA-15 for heterogeneous oxidation of phenol with sulfate radical for wastewater treatment, *Catal. Today* 175 (1) (2011) 380–385.
- [42] X. Duan, C. Su, L. Zhou, H. Sun, A. Suvorova, T. Odedairo, Z. Zhu, Z. Shao, S. Wang, Surface controlled generation of reactive radicals from persulfate by carbocatalysis on nanodiamonds, *Appl. Catal. B-Environ.* 194 (2016) 7–15.
- [43] Y.-C. Lee, S.-L. Lo, J. Kuo, Y.-L. Lin, Persulfate oxidation of perfluorooctanoic acid under the temperatures of 20–40 degrees C, *Chem. Eng. J.* 198 (2012) 27–32.
- [44] Y. Feng, D. Wu, Y. Deng, T. Zhang, K. Shih, Sulfate radical-mediated degradation of sulfadiazine by CuFeO<sub>2</sub> rhombohedral crystal-catalyzed peroxymonosulfate: synergistic effects and mechanisms, *Environ. Sci. Technol.* 50 (6) (2016) 3119–3127.
- [45] M.A. Al-Shamsi, N.R. Thomson, Treatment of organic compounds by activated persulfate using nanoscale zerovalent iron, *Ind. Eng. Chem. Res.* 52 (38) (2013) 13564–13571.
- [46] G.-D. Fang, D.D. Dionysiou, Y. Wang, S.R. Al-Abed, D.-M. Zhou, Sulfate radical-based degradation of polychlorinated biphenyls: effects of chloride ion and reaction kinetics, *J. Hazard. Mater.* 227 (2012) 394–401.
- [47] S. Dhaka, R. Kumar, S.-H. Lee, M.B. Kurade, B.-H. Jeon, Degradation of ethyl paraben in aqueous medium using advanced oxidation processes: efficiency evaluation of UV-C supported oxidants, *J. Cleaner Prod.* 180 (2018) 505–513.
- [48] M. Ahmadi, F. Ghanbari, A. Alvarez, S. Silva Martinez, UV-LEDs assisted peroxymonosulfate/Fe<sup>2+</sup> for oxidative removal of carmoisine: the effect of chloride ion, *Korean J. Chem. Eng.* 34 (8) (2017) 2154–2161.
- [49] C. Ding, S. Xiao, Y. Lin, P. Yu, M.-E. Zhong, L. Yang, H. Wang, L. Su, C. Liao, Y. Zhou, Y. Deng, D. Gong, Attapulgitite-supported nano-Fe<sub>0</sub>/peroxymonosulfate for quinclorac removal: performance, mechanism and degradation pathway, *Chem. Eng. J.* 360 (2019) 104–114.
- [50] X. Duan, Z. Ao, L. Zhou, H. Sun, G. Wang, S. Wang, Occurrence of radical and nonradical pathways from carbocatalysts for aqueous and nonaqueous catalytic oxidation, *Appl. Catal. B-Environ.* 188 (2016) 98–105.
- [51] D. Zhang, Y.-X. Wang, H.-Y. Niu, Z.-F. Meng, Degradation of norfloxacin by nano-Fe<sub>3</sub>O<sub>4</sub>/H<sub>2</sub>O<sub>2</sub>, *Huan jing ke xue=, Huanjing Kexue* 32 (10) (2011) 2943–2948.
- [52] J. Cao, S. Sun, X. Li, Z. Yang, W. Xiong, Y. Wu, M. Jia, Y. Zhou, C. Zhou, Y. Zhang, Efficient charge transfer in aluminum-cobalt layered double hydroxide derived from Co-ZIF for enhanced catalytic degradation of tetracycline through peroxymonosulfate activation, *Chem. Eng. J.* 382 (2020).
- [53] C. Gong, F. Chen, Q. Yang, K. Luo, F. Yao, S. Wang, X. Wang, J. Wu, X. Li, D. Wang, G. Zeng, Heterogeneous activation of peroxymonosulfate by Fe-Co layered double hydroxide for efficient catalytic degradation of Rhodamine B, *Chem. Eng. J.* 321 (2017) 222–232.
- [54] Q. Yang, X. Yang, Y. Yan, C. Sun, H. Wu, J. He, D. Wang, Heterogeneous activation of peroxymonosulfate by different ferromanganese oxides for tetracycline degradation: structure dependence and catalytic mechanism, *Chem. Eng. J.* 348 (2018) 263–270.
- [55] C. Wang, J. Kang, P. Liang, H. Zhang, H. Sun, M.O. Tade, S. Wang, Ferric carbide nanocrystals encapsulated in nitrogen-doped carbon nanotubes as an outstanding environmental catalyst, *Environ. Sci.-Nano* 4 (1) (2017) 170–179.
- [56] F. Gong, L. Wang, D. Li, F. Zhou, Y. Yao, W. Lu, S. Huang, W. Chen, An effective heterogeneous iron-based catalyst to activate peroxymonosulfate for organic contaminants removal, *Chem. Eng. J.* 267 (2015) 102–110.
- [57] Y. Hua, S. Wang, J. Xiao, C. Cui, C. Wang, Preparation and characterization of Fe<sub>3</sub>O<sub>4</sub>/gallic acid/graphene oxide magnetic nanocomposites as highly efficient Fenton catalysts, *RSC Adv.* 7 (46) (2017) 28979–28986.
- [58] J. Du, J. Bao, Y. Liu, S.H. Kim, D.D. Dionysiou, Facile preparation of porous Mn/Fe<sub>3</sub>O<sub>4</sub> cubes as peroxymonosulfate activating catalyst for effective bisphenol A degradation, *Chem. Eng. J.* 376 (2019).
- [59] L. Xie, Y. Zhong, R. Xiang, G. Fu, Y. Xu, Y. Cheng, Z. Liu, T. Wen, Y. Zhao, X. Liu, Sono-assisted preparation of Fe(II)-Al(III) layered double hydroxides and their application for removing uranium (VI), *Chem. Eng. J.* 328 (2017) 574–584.
- [60] S. Yang, T. Xiao, J. Zhang, Y. Chen, L. Li, Activated carbon fiber as heterogeneous catalyst of peroxymonosulfate activation for efficient degradation of Acid Orange 7 in aqueous solution, *Separ. Purif. Technol.* 143 (2015) 19–26.
- [61] G.-X. Huang, C.-Y. Wang, C.-W. Yang, P.-C. Guo, H.-Q. Yu, Degradation of bisphenol A by peroxymonosulfate catalytically activated with Mn<sub>1.8</sub>Fe<sub>1.2</sub>O<sub>4</sub> nanospheres: synergism between Mn and Fe, *Environ. Sci. Technol.* 51 (21) (2017) 12611–12618.
- [62] X. Qiu, S. Yang, M. Dzakpasu, X. Li, D. Ding, P. Jin, R. Chen, Q. Zhang, X.C. Wang, Attenuation of BPA degradation by SO<sub>4</sub> center dot- in a system of peroxymonosulfate coupled with Mn/Fe MOF-templated catalysts and its synergism with Cl<sup>-</sup> and bicarbonate, *Chem. Eng. J.* 372 (2019) 605–615.
- [63] M. Carrier, C. Guillard, M. Besson, C. Bordes, H. Chermette, Photocatalytic degradation of diuron: experimental analyses and simulation of HO degrees radical attacks by density functional theory calculations, *J. Phys. Chem. A* 113 (22) (2009) 6365–6374.
- [64] T. An, H. Yang, G. Li, W. Song, X. Nie, Kinetics and mechanism of advanced oxidation processes (AOPs) in degradation of ciprofloxacin in water, *Appl. Catal. B* 94 (3) (2010) 288–294.